Modeling and analysis of nonlinear rotordynamics due to higher order deformations in bending

Muhammad Rizwan Shad [a,*], Guilhem Michon [b,1], Alain Berlioz [c,2]

[a] Université de Toulouse, ICA, INSA, 135 Av. Rangueil, 31077 Toulouse, France
[b] Université de Toulouse, ICA, ISAE, 10 Av. Edouard Belin, 31055 Toulouse, France
[c] Université de Toulouse, ICA, UPS, 118 Route de Narbonne, 31062 Toulouse, France

ABSTRACT

A mathematical model incorporating the higher order deformations in bending is developed and analyzed to investigate the nonlinear dynamics of rotors. The rotor system considered for the present work consists of a flexible shaft and a rigid disk. The shaft is modeled as a beam with a circular cross section and the Euler Bernoulli beam theory is applied with added effects such as rotary inertia, gyroscopic effect, higher order large deformations, rotor mass unbalance and dynamic axial force. The kinetic and strain (deformation) energies of the rotor system are derived and the Rayleigh–Ritz method is used to discretize these energy expressions. Hamilton's principle is then applied to obtain the mathematical model consisting of second order coupled nonlinear differential equations of motion. In order to solve these equations and hence obtain the nonlinear dynamic response of the rotor system, the method of multiple scales is applied. Furthermore, this response is examined for different possible resonant conditions and resonant curves are plotted and discussed. It is concluded that nonlinearity due to higher order deformations significantly affects the dynamic behavior of the rotor system leading to resonant hard spring type curves. It is also observed that variations in the values of different parameters like mass unbalance and shaft diameter greatly influence dynamic response. These influences are also presented graphically and discussed.

1. Introduction

Over the years rotordynamics has become an important field in many engineering applications [1–3] such as jet engines, helicopter rotors, turbines, compressors and the spindles of machine tools, etc. The prediction and analysis of the dynamic behavior of rotor systems [4,5] are crucial because their rotating components possess unlimited amounts of energy that can be transformed into vibrations. However, these vibrations can disturb the performance of the rotor system and even cause its total destruction. The importance of considering the nonlinear and/or material constitution [6] effects in the dynamic analysis of rotating equipment has increased in line with current demand for accurate and optimized performance. Thus this field has become more challenging because the analysis of the nonlinear phenomena is far more difficult in comparison to linear analysis. Nonlinearities in rotor systems can be due to many reasons [7]. For example, higher order large deformations, rotor-base excitations [8–10], geometric nonlinearities [11,12], oil film in journal bearings [13], magnetic bearings [14].

This article investigates the dynamics of the rotor system analytically and numerically, by considering nonlinearity due to higher order large deformations in bending. In addition, if the supports of the rotor do not allow the shaft to move in the axial direction, then dynamic force will act on the rotor axially as it operates [15]. This force will also produce large deformations in bending. Moreover, there are other secondary effects that should be considered for increasing the accuracy of the predicted results. These include rotary inertia effects, gyroscopic effects and rotor mass unbalance effects.

In order to include the above-mentioned effects in the analysis of rotordynamics, a nonlinear mathematical model has been developed. Hamilton's principle [16] is used to formulate the equations of motion. The linear part of the model developed is analyzed for the first mode to obtain the natural frequencies of vibrations. In addition, the Campbell diagram is plotted to determine the critical speeds and the system response due to an unbalanced mass. Then, in order to solve the complete model including nonlinear terms, the method of multiple scales (MMS) [17] is applied. This is a well known perturbation method [18] and has been proven to be very effective for solving nonlinear equations of motion [19–22]. Resonant curves are plotted for different possible resonances and the effect of nonlinearity is discussed in comparison to the linear analysis. The forced response of the rotor system due to an unbalanced mass by changing different rotor parameters is also presented and the results are plotted graphically and discussed.

2. Modeling

The rotor system considered for this work consists of a flexible shaft and a rigid disk. We selected the same rotor geometry as used by Duchemin et al. [9,10] shown in Fig. 1. The shaft, considered to be a beam of circular cross section of length L and radius R_1, is modeled by its kinetic and strain energies. The disk of external radius R_2 and internal radius R_1 positioned at a distance $y = L/3$, is considered to be rigid and hence only requires kinetic energy for its characterization. The mass unbalance denoted by m_u is also situated at a distance $y = L/3$.

2.1. Kinetic energy

The kinetic energies of the disk, shaft and mass unbalance, denoted by T_d, T_s and T_u respectively, are given according to [3]

$$T_d = \frac{M_d}{2}(\dot{u}^2 + \dot{w}^2) + \frac{I_{dx}}{2}\left(\dot{\theta}_x^2 + \dot{\theta}_z^2\right) + I_{dy}\Omega\dot{\theta}_z\theta_x, \tag{1}$$
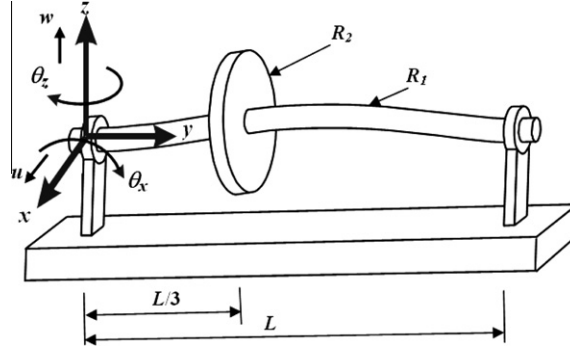
Fig. 1. Rotor with shaft and disk.

$$T_s = \int_0^L \frac{\rho I}{2}\left(\dot{\theta}_x^2 + \dot{\theta}_z^2\right)dy + \int_0^L \frac{\rho A}{2}(\dot{u}^2 + \dot{w}^2)dy + \int_0^L 2\rho I\Omega\dot{\theta}_z\theta_x dy, \tag{2}$$

$$T_u = m_u\Omega d_1(\dot{u}\cos\Omega t - \dot{w}\sin\Omega t). \tag{3}$$

By adding Eqs. (1)–(3) the total kinetic energy of the rotor system becomes $T_R = T_d + T_s + T_u$.

2.2. Strain energy

The following expression for the strain energy of the shaft taking into account higher order large deformations is derived in Appendix A.

$$U_{s1} = \int_0^L \frac{EI}{2}\left\{\left(\frac{\partial\theta_x}{\partial y}\right)^2 + \left(\frac{\partial\theta_z}{\partial y}\right)^2\right\}dy + \int_0^L \frac{EA}{2}\left(\frac{1}{4}\theta_x^4 + \frac{1}{4}\theta_z^4 + \frac{1}{2}\theta_x^2\theta_z^2\right)dy. \tag{4}$$

If the supports at both ends of the shaft are such that they do not allow the shaft to elongate, then an axial force N_A will act dynamically on the shaft. This force leads to another contribution to the strain energy of the shaft given by $U_{s2} = \frac{N_A}{2}\int_0^L (\theta_x^2 + \theta_z^2)dy$ where N_A can be shown to be $N_A = \int_0^L \frac{EA}{2L}(\theta_x^2 + \theta_z^2)dy$. Therefore, the strain energy of the shaft becomes $U_s = U_{s1} + U_{s2}$ and is given by

$$U_s = \int_0^L \left\{\frac{EI}{2}\left(\frac{\partial\theta_x}{\partial y}\right)^2 + \left(\frac{\partial\theta_z}{\partial y}\right)^2\right\}dy + \int_0^L \frac{EA}{2}\left(\frac{1}{4}\theta_x^4 + \frac{1}{4}\theta_z^4 + \frac{1}{2}\theta_x^2\theta_z^2\right)dy + \int_0^L \int_0^L \frac{EA}{4L}(\theta_x^2 + \theta_z^2)dy(\theta_x^2 + \theta_z^2)dy. \tag{5}$$

The total strain energy of the rotor system can now be written as $U_R = U_s$

2.3. Application of the Rayleigh–Ritz method

The displacements in the x and z directions can be expressed as,

$$u(y,t) = f(y)U(t) = f(y)U \text{ and } w(y,t) = f(y)W(t) = f(y)W. \tag{6}$$

The angular displacements can be approximated as

$$\theta_x = \partial w/\partial y = f'(y)W = g(y)W, \quad \partial\theta_x/\partial y = f''(y)W = h(y)W, \tag{7a}$$

$$\theta_z = -\partial u/\partial y = -f'(y)U = -g(y)U, \quad \partial\theta_z/\partial y = -f''(y)U = -h(y)U, \tag{7b}$$

where the prime denotes the derivative with respect to y. Using the expressions given by Eqs. (6), (7a) and (7b), the kinetic energy of the rotor system in a compact form can be given as,

$$T_R = \frac{1}{2}b_1\left(\dot{U}^2 + \dot{W}^2\right) - \Omega b_2\dot{U}W + m_u\Omega d_1 f(l_1)(\dot{U}\cos\Omega t - \dot{W}\sin\Omega t), \tag{8}$$

where,

$$b_1 = M_D f^2(l_1) + I_{Dx}g^2(l_1) + \rho A\int_0^L f^2(y)dy + \rho I\int_0^L g^2(y)dy, \tag{9a}$$

$$b_2 = I_{Dy}g^2(l_1) + 2\rho I\int_0^L g^2(y)dy. \tag{9b}$$

The strain energy of the rotor in a compact form can be written as,

$$U_R = \frac{k_1}{2}\left(U^2 + W^2\right) + \frac{k_2}{8}\left(U^4 + W^4 + 2U^2W^2\right) + \frac{k_3}{4}\left(U^4 + W^4 + 2U^2W^2\right), \tag{10}$$

where,

$$k_1 = EI \int_0^L h^2(y)dy; \quad k_2 = EA \int_0^L g^4(y)dy; \quad k_3 = \frac{EA}{L}\int_0^L \int_0^L h^4(y)dydy. \tag{11}$$

2.4. Application of the Hamilton principle

Using the Hamilton principle as $\int_{t_1}^{t_2} \delta(T_R - U_R)dt = 0$, we can write

$$\int_{t_1}^{t_2} \delta(T_R - U_R)dt = \int_{t_1}^{t_2} \delta T_R dt - \int_{t_1}^{t_2} \delta U_R dt = 0. \tag{12}$$

We will treat the two terms in Eq. (12) one by one. The first term gives

$$\int_{t_1}^{t_2} \delta T_R dt = \int_{t_1}^{t_2}\left[\frac{\partial T_R}{\partial W}\delta W + \frac{\partial T_R}{\partial \dot{U}}\delta \dot{U} + \frac{\partial T_R}{\partial \dot{W}}\delta \dot{W}\right]dt. \tag{13}$$

Different terms in Eq. (13) can be calculated as follows

$$\int_{t_1}^{t_2} \frac{\partial T_R}{\partial W}\delta W dt = -\int_{t_1}^{t_2} \Omega b_2 \dot{U}\delta W dt, \tag{14a}$$

$$\int_{t_1}^{t_2} \frac{\partial T_R}{\partial \dot{U}}\delta \dot{U} dt = \left[\frac{\partial T_R}{\partial \dot{U}}\delta U\right]_{t_1}^{t_2} - \int_{t_1}^{t_2} \frac{\partial}{\partial t}\left(\frac{\partial T_R}{\partial \dot{U}}\right)\delta U dt = \left[\frac{\partial T_R}{\partial \dot{U}}\delta U\right]_{t_1}^{t_2} - \int_{t_1}^{t_2} \frac{\partial}{\partial t}(b_1\dot{U} - \Omega b_2 W + m_u\Omega d_1 f(l_1)\cos\Omega t)\delta U dt, \tag{14b}$$

$$\int_{t_1}^{t_2} \frac{\partial T_R}{\partial \dot{W}}\delta \dot{W} dt = \left[\frac{\partial T_R}{\partial \dot{W}}\delta W\right]_{t_1}^{t_2} - \int_{t_1}^{t_2} \frac{\partial}{\partial t}\left(\frac{\partial T_R}{\partial \dot{W}}\right)\delta W dt = \left[\frac{\partial T_R}{\partial \dot{W}}\delta W\right]_{t_1}^{t_2} - \int_{t_1}^{t_2} \frac{\partial}{\partial t}\left(b_1\dot{W} - m_u\Omega d_1 f(l_1)\sin\Omega t\right)\delta W dt. \tag{14c}$$

Similarly, the second term in Eq. (12) gives

$$\int_{t_1}^{t_2} \delta U_R dt = \int_{t_1}^{t_2}\left[\frac{\partial U_R}{\partial U}\delta U + \frac{\partial U_R}{\partial W}\delta W\right]dt. \tag{15}$$

The two terms in Eq. (15) can be written as below

$$\int_{t_1}^{t_2} \frac{\partial U_R}{\partial U}\delta U dt = \int_{t_1}^{t_2}\left[k_1 U + \left(\frac{1}{2}k_2 + k_3\right)(U^3 + UW^2)\right]\delta U dt, \tag{16a}$$

$$\int_{t_1}^{t_2} \frac{\partial U_R}{\partial W}\delta W dt = \int_{t_1}^{t_2}\left[k_1 W + \left(\frac{1}{2}k_2 + k_3\right)\left(W^3 + U^2 W\right)\right]\delta W dt, \tag{16b}$$

The equations of motion can be written by collecting the terms of type $\delta U dt$ and $\delta W dt$ in Eqs. (14a)–(14c), and (16a), (16b).

2.4.1. For δU

$$-\int_{t_1}^{t_2}\left[\begin{array}{l}\frac{\partial}{\partial t}\left(b_1\dot{U} - \Omega b_2 W + m_u\Omega d_1 f(l_1)\cos\Omega t\right) - k_1 U \\ -(\frac{1}{2}k_2 + k_3)(U^3 + UW^2)\end{array}\right]\delta U dt = 0. \tag{17}$$

By simplifying and rearranging Eq. (17) we can write,

$$b_1\ddot{U} - \Omega b_2\dot{W} + k_1 U + \left(\frac{1}{2}k_2 + k_3\right)(U^3 + UW^2) = m_u\Omega^2 d_1 f(l_1)\sin\Omega t. \tag{18}$$

*2.4.2. For δ**W***

$$-\int_{t_1}^{t_2} \left[\begin{matrix} \frac{\partial}{\partial t}\left(b_1\dot{W} - m_u\Omega d_1 f(l_1)\sin\Omega t\right) - \Omega b_2\dot{U} - k_1 W \\ -\left(\frac{1}{2}k_2 + k_3\right)(W^3 + U^2 W) \end{matrix} \right] \delta W dt = 0. \tag{19}$$

By simplifying and rearranging Eq. (19) we can write,

$$b_1\ddot{W} + \Omega b_2\dot{U} + k_1 W + \left(\frac{1}{2}k_2 + k_3\right)(W^3 + U^2 W) = m_u\Omega^2 d_1 f(l_1)\cos\Omega t. \tag{20}$$

Eqs. (18) and (20) can then be written as

$$\ddot{U} - \Omega\alpha_1\dot{W} + \alpha_2 U + \left(\frac{1}{2}\beta_1 + \beta_2\right)(U^3 + UW^2) + c\dot{U} = m_1\Omega^2 d_1 f(l_1)\sin\Omega t, \tag{21a}$$

$$\ddot{W} + \Omega\alpha_1\dot{U} + \alpha_2 W + \left(\frac{1}{2}\beta_1 + \beta_2\right)(W^3 + WU^2) + c\dot{W} = m_1\Omega^2 d_1 f(l_1)\cos\Omega t. \tag{21b}$$

Eqs. (21a) and (21b) are two nonlinear second order differential equations of motion of the rotor system studied, where a damping term c has been added Also

$$\alpha_1 = b_2/b_1, \quad \alpha_2 = k_1/b_1, \quad \beta_1 = k_2/b_1, \quad \beta_2 = k_3/b_1, \quad m_1 = m_u/b_1. \tag{22}$$

The analysis of the free undamped linear system is similar to [3]. The Campbell diagram, forced response of the linear system and numerical data are presented in Appendix B.

3. Nonlinear analysis

The theoretical analysis of the nonlinear forced system is performed using the method of multiple scales in time (MMS), which has been proven very effective in the analysis of such systems [17–22]. In order to apply MMS, displacements U and W are expanded as below

$$U(T_0, T_1) = u_0(T_0, T_1) + \varepsilon u_1(T_0, T_1) = u_0 + \varepsilon u_1, \tag{23a}$$

$$W(T_0, T_1) = w_0(T_0, T_1) + \varepsilon w_1(T_0, T_1) = w_0 + \varepsilon w_1, \tag{23b}$$

where $T_n = \varepsilon^n t$ are slow time scales, T_1 being slower than T_0, and ε is a small dimensionless parameter so that $\varepsilon << 1$. The nonlinear, damping and forcing terms in Eqs. (21a) and (21b) are scaled so that they appear in the same order of ε. Therefore the following scaling is used

$$\alpha_1 = \alpha_1, \quad \alpha_2 = \alpha_2, \quad \beta_1 = \varepsilon\beta_1, \quad \beta_2 = \varepsilon\beta_2, \quad m_1 = \varepsilon m_1, \quad c = \varepsilon c. \tag{24}$$

Eqs. (21a) and (21b) can now be written as

$$\ddot{U} - \Omega\alpha_1\dot{W} + \alpha_2 U + \varepsilon\left(\frac{1}{2}\beta_1 + \beta_2\right)\left(U^3 + UW^2\right) + \varepsilon c\dot{U} = \varepsilon m_1\Omega^2 d_1 f(l_1)\sin\Omega t, \tag{25a}$$

$$\ddot{W} + \Omega\alpha_1\dot{U} + \alpha_2 W + \varepsilon\left(\frac{1}{2}\beta_1 + \beta_2\right)\left(W^3 + WU^2\right) + \varepsilon c\dot{W} = \varepsilon m_1\Omega^2 d_1 f(l_1)\cos\Omega t. \tag{25b}$$

The different time derivatives in the above equation can now be written as:

$$\dot{U}(t) = \frac{\partial}{\partial T_0}U(T_0, T_1) + \varepsilon\frac{\partial}{\partial T_1}U(T_0, T_1), \tag{26a}$$

$$\dot{W}(t) = \frac{\partial}{\partial T_0}W(T_0, T_1) + \varepsilon\frac{\partial}{\partial T_1}W(T_0, T_1), \tag{26b}$$

$$\ddot{U}(t) = \frac{\partial^2}{\partial T_0^2}U(T_0, T_1) + 2\varepsilon\frac{\partial^2}{\partial T_0\partial T_1}U(T_0, T_1), \tag{26c}$$

$$\ddot{W}(t) = \frac{\partial^2}{\partial T_0^2}W(T_0, T_1) + 2\varepsilon\frac{\partial^2}{\partial T_0\partial T_1}W(T_0, T_1). \tag{26d}$$

By substituting Eqs. (26a)–(26d) in Eqs. (25a) and (25b), using Eqs. (23a) and (23b) and then equating the coefficients of the like powers of ε on both sides of the resulting equations, we obtain following two systems of equations

System of order 0 equations (ε^0)

$$\frac{\partial^2}{\partial T_0^2}u_0 + \alpha_2 u_0 - \Omega\alpha_1\frac{\partial}{\partial T_0}w_0 = 0, \tag{27a}$$

$$\frac{\partial^2}{\partial T_0^2}w_0 + \alpha_2 w_0 - \Omega\alpha_1\frac{\partial}{\partial T_0}u_0 = 0. \tag{27b}$$

System of order 1 equations (ε^1)

$$\frac{\partial^2}{\partial T_0^2}u_1 + \alpha_2 u_1 - \Omega\alpha_1\frac{\partial}{\partial T_0}w_1 = \Omega\alpha_1\frac{\partial}{\partial T_0}w_0 - 2\frac{\partial^2}{\partial T_0\partial T_1}u_0 - \frac{\beta_1 u_0^3}{2} - \frac{\beta_1 u_0 w_0^2}{2} - \beta_2 u_0^3 - \beta_2 u_0 w_0^2 - c\frac{\partial}{\partial T_0}u_0 + m_1\Omega^2 d_1 f(l_1)\sin\Omega t, \tag{28a}$$

$$\frac{\partial^2}{\partial T_0^2}w_1 + \alpha_2 w_1 + \Omega\alpha_1\frac{\partial}{\partial T_0}u_1 = -\Omega\alpha_1\frac{\partial}{\partial T_0}u_0 - 2\frac{\partial^2}{\partial T_0\partial T_1}w_0 - \frac{\beta_1 w_0^3}{2} - \frac{\beta_1 w_0 u_0^2}{2} - \beta_2 w_0^3 - \beta_2 w_0 u_0^2 - c\frac{\partial}{\partial T_0}w_0$$
$$+ m_1\Omega^2 d_1 f(l_1)\cos\Omega t. \tag{28b}$$

The solution of Eqs. (27a) and (27b) is given as

$$u_0 = A_1(T_1)\exp(i\omega_1 T_0) + A_2(T_1)\exp(i\omega_2 T_0) + [cc], \tag{29a}$$

$$w_0 = iA_1(T_1)\exp(i\omega_1 T_0) - iA_2(T_1)\exp(i\omega_2 T_0) + [cc], \tag{29b}$$

where [cc] denotes the complex conjugate.

3.1. Possible resonances and solvability conditions

Substitution of Eqs. (29a) and (29b) into Eqs. (28a) and (28b) gives us the following two equations

$$\frac{\partial^2 u_1}{\partial T_0^2} + \alpha_2 u_1 - \Omega\alpha_1\frac{\partial}{\partial T_0}w_1 = \left(-2i\omega_1\frac{\partial A_1}{\partial T_1} + i\alpha_1\Omega\frac{\partial A_1}{\partial T_1} - ic\omega_1 A_1 - 2\beta_1 A_1^2\overline{A_1} - 4\beta_2 A_1^2\overline{A_1} - 4\beta_1 A_1 A_2\overline{A_2} - 8\beta_2 A_1 A_2\overline{A_2}\right)\exp(i\omega_1 T_0)$$
$$- \left(2i\omega_2\frac{\partial A_2}{\partial T_1} + i\alpha_1\Omega\frac{\partial A_2}{\partial T_1} + icA_2\omega_2 + 2\beta_1 A_2^2\overline{A_2} + 4\beta_2 A_2^2\overline{A_2} + 4\beta_1 A_1\overline{A_1}A_2 + 8\beta_2 A_1\overline{A_1}A_2\right)\exp(i\omega_2 T_0)$$
$$- \frac{1}{2}im_1\Omega^2 d_1 f(l_1)\exp(i\Omega T_0) - \left(2\beta_1 A_1 A_2^2 + 4\beta_2 A_1 A_2^2\right)\exp(i(\omega_1 + 2\omega_2)T_0)$$
$$- \left(2\beta_1 A_1^2 A_2 + 4\beta_2 A_1^2 A_2\right)\exp(i(2\omega_1 + \omega_2)T_0) + [cc], \tag{30a}$$

$$\frac{\partial^2 w_1}{\partial T_0^2} + \alpha_2 w_1 + \Omega\alpha_1\frac{\partial}{\partial T_0}u_1 = \left(-2\omega_1\frac{\partial A_1}{\partial T_1} - \alpha_1\Omega\frac{\partial A_1}{\partial T_1} + c\omega_1 A_1 - 2i\beta_1 A_1^2\overline{A_1} - 4i\beta_2 A_1^2\overline{A_1} - 4i\beta_1 A_1 A_2\overline{A_2} - 8i\beta_2 A_1 A_2\overline{A_2}\right)\exp(i\omega_1 T_0)$$
$$- \left(2\omega_2\frac{\partial A_2}{\partial T_1} + \alpha_1\Omega\frac{\partial A_2}{\partial T_1} + c\omega_2 A_2 - 2i\beta_1 A_2^2\overline{A_2} - 4i\beta_2 A_2^2\overline{A_2} - 8i\beta_2 A_1\overline{A_1}A_2 - 4i\beta_1 A_1\overline{A_1}A_2\right)\exp(i\omega_2 T_0)$$
$$+ \frac{1}{2}m_1\Omega^2 d_1 f(l_1)\exp(i\Omega T_0) + \left(2i\beta_1 A_1 A_2^2 + 4i\beta_2 A_1 A_2^2\right)\exp(i(\omega_1 + 2\omega_2)T_0)$$
$$- \left(2i\beta_1 A_1^2 A_2 + 4i\beta_2 A_1^2 A_2\right)\exp(i(2\omega_1 + \omega_2)T_0) + [cc]. \tag{30b}$$

We assume a particular solution in the form:

$$u_1 = P_1(T_1)\exp(i\omega_1 T_0) + Q_1(T_1)\exp(i\omega_2 T_0), \tag{31a}$$

$$w_1 = P_2(T_1)\exp(i\omega_1 T_0) + Q_2(T_1)\exp(i\omega_2 T_0). \tag{31b}$$

After substituting the particular solution given above in Eqs. (30a) and (30b), it can be observed from the resulting equations that there are two possible primary resonance conditions, $\Omega = \omega_1$ and $\Omega = \omega_2$.

3.2. Case of $\Omega = \omega_2$

For this case we have used $\Omega = \omega_2 + \varepsilon\sigma_1$, where σ_1 is a detuning parameter for controlling the nearness of Ω to ω_2.

Also, the solutions of Eqs. (30a) and (30b) exist only if certain solvability conditions are satisfied. The first step in determining these solvability conditions is to substitute $\Omega = \omega_2 + \varepsilon\sigma_1$ and the particular solution, given in Eqs. (31a) and (31b), in these equations. We then equate the coefficients of $\exp(i\omega_1 T_0)$ and $\exp(i\omega_2 T_0)$ on both sides of the resulting equations and follow the procedure given in [17] to determine the solvability conditions.
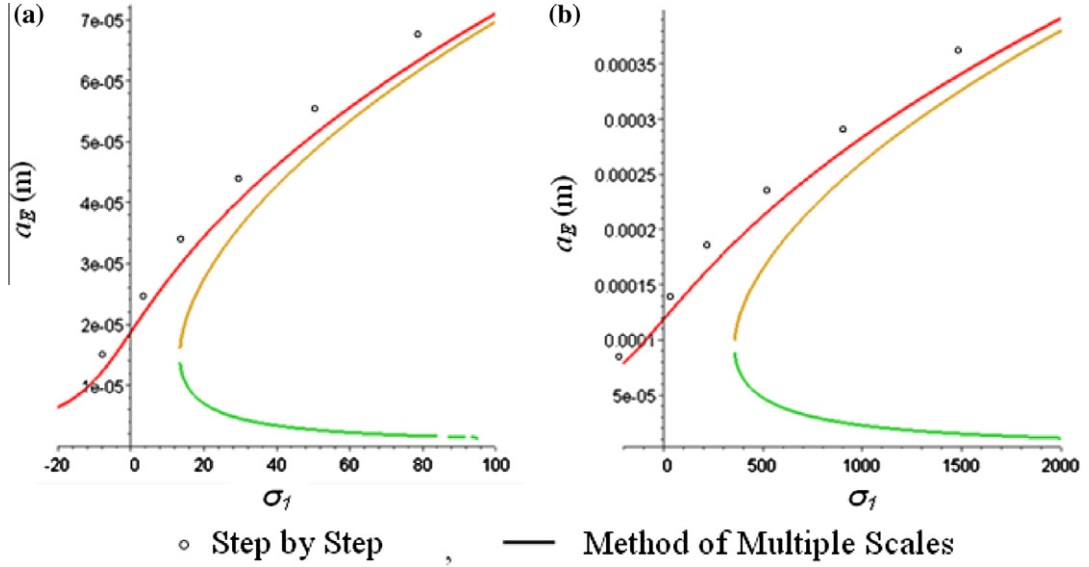
Fig. 2. Resonance curves (a) $\Omega = \omega_1$ (b) $\Omega = \omega_2$.

Finally, two solvability conditions are given below

$$\frac{\partial A_1}{\partial T_1} = -c_2 A_1^2 \overline{A_1} - c_3 A_1 A_2 \overline{A_2} - c_5 A_1, \tag{32a}$$

$$\frac{\partial A_2}{\partial T_1} = -d_2 A_2^2 \overline{A_2} - d_3 A_1 \overline{A_1} A_2 - d_4 \exp(i\sigma_1 T_1) - d_5 A_2, \tag{32b}$$

where $c_2, c_3, c_5, d_3, d_4, d_5$ are constants, given in Appendix B.

Substituting the solutions of A_1 and A_2 in the polar form i.e., $A_n = (1/2)(a_n \exp(i\theta_n)$ where $n = 1, \dots, 2$, in Eqs. (32a) and (32b) and separating the real and imaginary parts we obtain the following autonomous system of four first order partial differential equations.

$$\frac{1}{2}\frac{\partial a_1}{\partial T_1} + \frac{1}{8}c_2 a_1^3 + \frac{1}{8}c_3 a_1 a_2^2 + \frac{1}{2}c_5 a_1 = 0, \tag{33a}$$

$$\frac{1}{2}a_1 \frac{\partial \theta_1}{\partial T_1} = 0, \tag{33b}$$

$$\frac{1}{2}\frac{\partial a_2}{\partial T_1} + \frac{1}{8}d_2 a_2^3 + \frac{1}{8}d_3 a_1^2 a_2 + d_4 \cos(\Gamma) + \frac{1}{2}d_5 a_2 = 0, \tag{33c}$$

$$-\frac{1}{2}a_2 \sigma_1 + \frac{1}{2}a_2 \frac{\partial \Gamma}{\partial T_1} - d_4 \sin(\Gamma) = 0, \tag{33d}$$

where $\Gamma = -\theta_2 + \sigma_1 T_1$.

Eqs. (33a) and (33b) show that $a_1 = 0$ is a solution. Equilibrium is also achieved in $\partial a_1/\partial T_1 = 0$, $\partial \Gamma / \partial T_1 = 0$. The autonomous system above now reduces to two equations that can be resolved to give the following 6th degree polynomial equation for plotting the resonant curves.

$$d_2^2 a_E^6 + 8 d_2 d_5 a_E^4 + 16(d_5^2 + \sigma_1^2)a_E^2 - 64 d_4^2 = 0. \tag{34}$$

The above polynomial is a function of amplitude at equilibrium a_E and detuning parameter σ_1. Solving this polynomial gives six solutions that are symbolically complicated expressions and are not reproduced here. Therefore this polynomial is treated numerically in the next section.
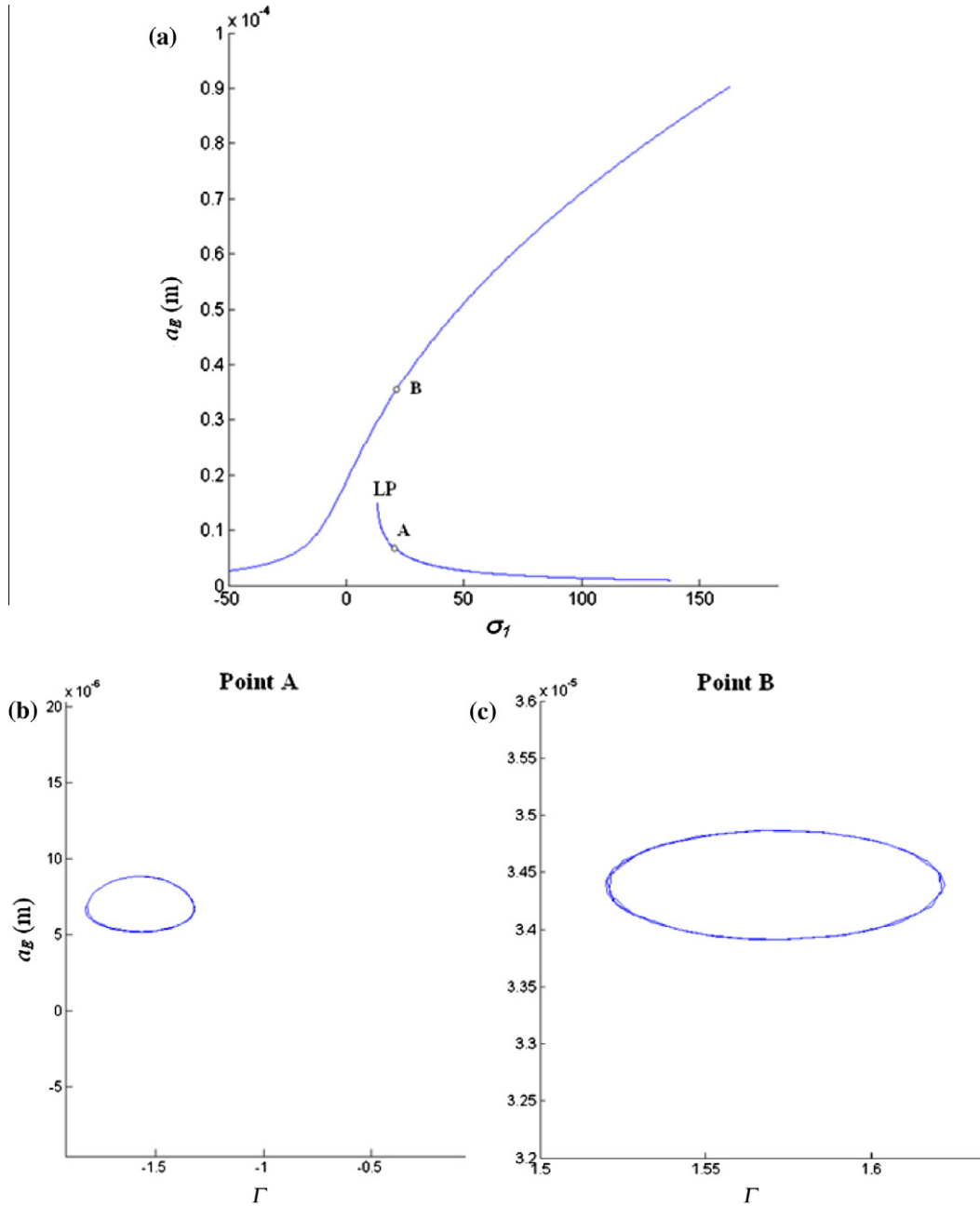
Fig. 3. Results obtained by continuation procedure using Matcont at $\sigma_1 = 20$ for bifurcation diagram, (b) state plane at point A, (c) state plane at point B.

3.3. Case of $\Omega = \omega_1$

This case can be treated in the same way as the previous one. The results can be obtained directly by changing ω_2 with ω_1 in Eqs. (30a) and (30b) and considering a new detuning parameter defined as $\Omega = \omega_1 + \varepsilon\sigma_1$.

4. Numerical investigations (Results and discussion)

The investigations were conducted using three different methods, i.e. the method of multiple scales, a continuation scheme in Matlab called Matcont[3] and a step by step integration method in Matlab Simulink. All the numerical data are given in Appendix B.

---

[3] A. Dhooge, W. Govaerts, Yu.A. Kuznetsov, W. Mestrom, A. M. Riet, B. Sautois, MATCONT: A continuation toolbox in Matlab, http://www.matcont.ugent.be/.
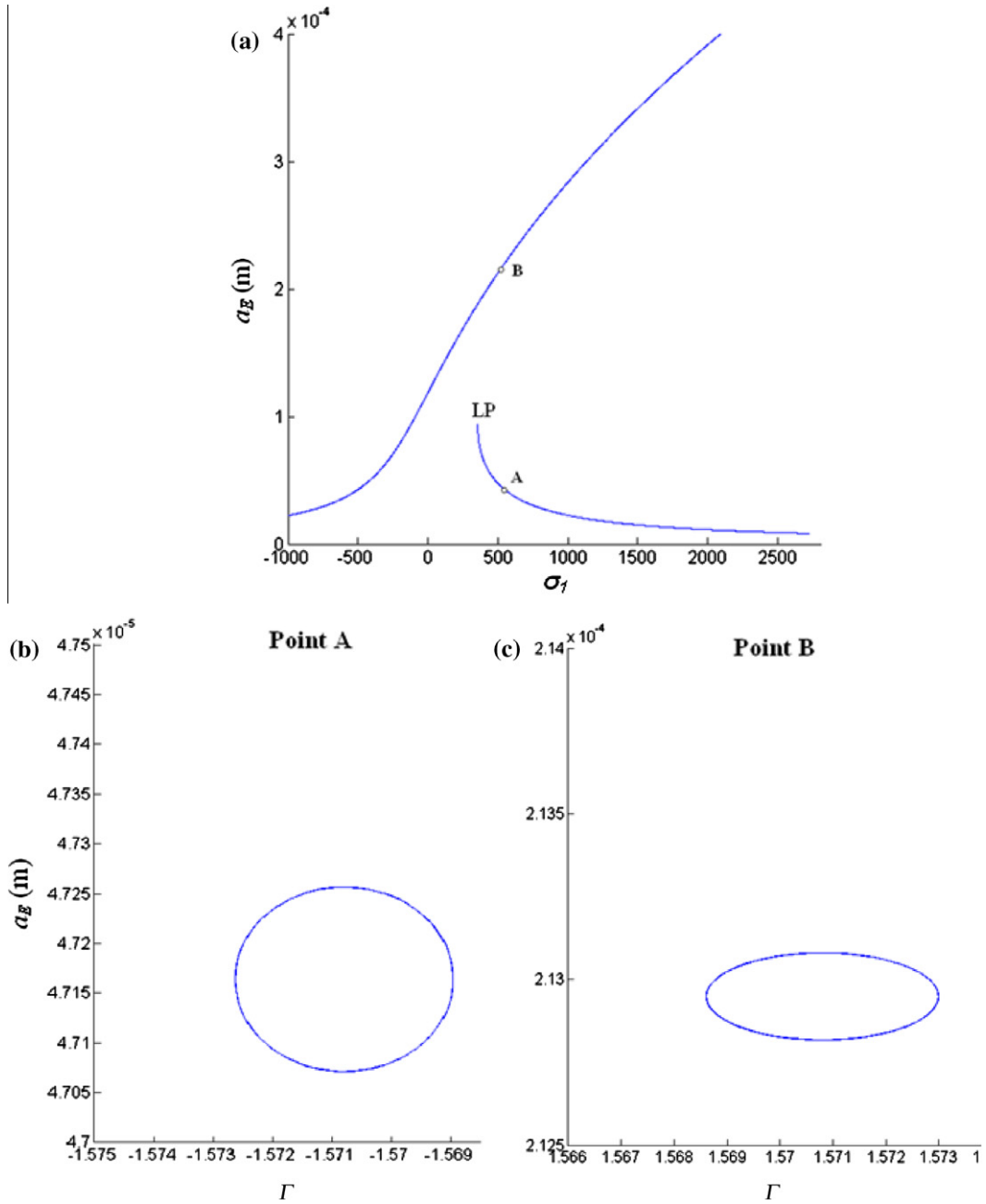
Fig. 4. Results obtained by continuation procedure using Matcont at $\sigma_1 = 504$ for $\Omega = \omega_2$ (a) bifurcation diagram, (b) state plane at point A, (c) state plane at point B.

4.1. Resonant curves

4.1.1. Method of multiple scales (MMS)

The numerical solutions for the two resonant conditions $\Omega = \omega_1$ and $\Omega = \omega_2$ are presented showing the plots of resonant curves of hard spring type (Fig. 2).

The effect of nonlinearity has caused these curves to bend rightwards from the position of the linear response given in Appendix B in Fig. B. It is interesting to note the plotting ranges of these curves to generate the same shapes. For the case $\Omega = \omega_2$ these curves are significantly expanded and the range of amplitude is higher.

4.1.2. Continuation procedure (Matcont)

The bifurcation diagrams and state planes are presented in Figs. 3 and 4. For a given value of the detuning parameter there are three solutions in the positive plane. Out of these solutions, two are stable and one is unstable. The continuation procedure is capable of tracing two stable solutions which can be seen corresponding to points A and B on the curves in Fig. 3(a) and Fig. 4(a). The curve of the unstable solution lies somewhere between these two curves. The results of this procedure match with those obtained by MMS but the latter is more preferable as it can plot the unstable solutions as well.

The state planes are plotted for two different points A and B on the resonant curves given in Fig. 3(a) and Fig. 4(a). It can be observed that the amplitude at point A is much lower as compared to that of point B. Also the orbits corresponding to point B tend to be more oval as compared to those corresponding to point A. Therefore it can be concluded that the effect of nonlinearity due to higher order deformations is more visible at the curve at point B.
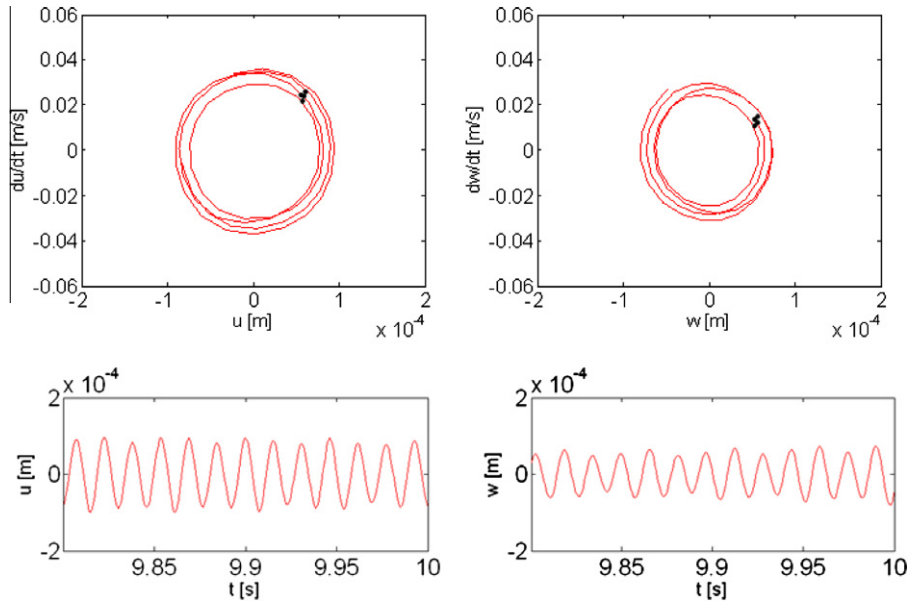

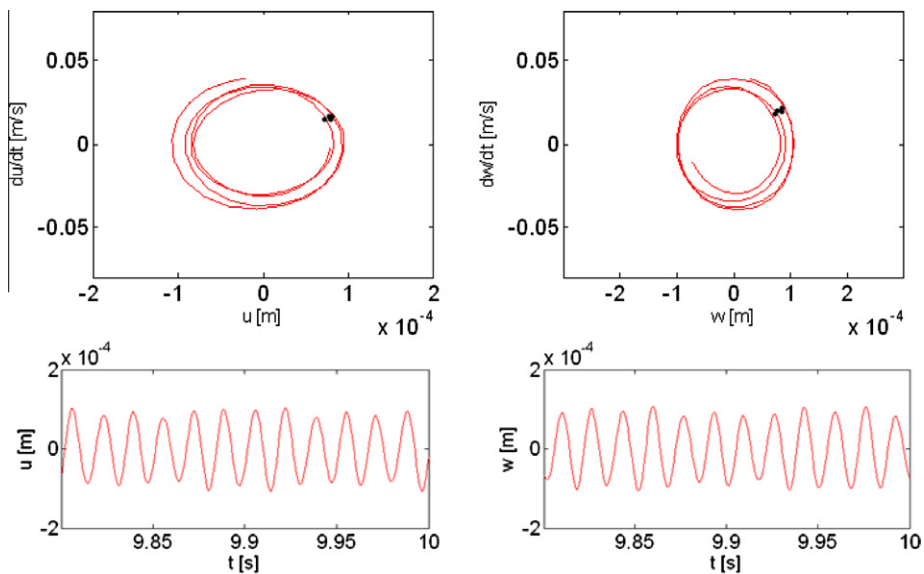**Fig. 5.** Phase diagrams, poincaré sections and time amplitude responses for $\Omega = \omega_1$.

Fig. 6. Phase diagrams, poincaré sections and time amplitude responses for $\Omega = \omega_2$.

4.1.3. Direct integration by step by step method (Matlab)

A step by step analysis was conducted using the Simulink toolbox of the Matlab. The equations of motion given by Eqs. (21a) and (21b) are treated directly. The results are compared with those obtained by MMS and are presented as dots in Fig. 2. The phase diagrams, poincaré sections and time histories of the amplitude are given in Figs. 5 and 6. The discrepancy between MMS results and step by step results in Fig. 2 are mainly due to the difficulty to obtain the maximum and minimum in the amplitude response curves, see for example Figs. 5 and 6. The amplitude modulation is also visible in these figures. The simulation was carried out and the phase diagrams were plotted for the last 0.2 s. This corresponds to 4 periods where the amplitude modulation is low. Hence as a result the 4 points on the poincaré sections lie close together.

4.2. Effect of various parameters

In regard to the limitations presented by the continuation procedure (the inefficiency in predicting unstable branch) and step by step method (difficulty in choosing the initial conditions and hence not attaining the stability in time amplitude response), in the following the method of multiple scales is used. In Eq. (34) d_2, d_4 and d_5 are functions of various quantities α_1, β_1, α_2, β_2 and m_1 (Appendix B). These quantities, according to Eqs. (22), (11), and (9a), (9b), further depend on geometric, material and mass unbalance parameters. This indicates that a change in the values of these parameters will give different
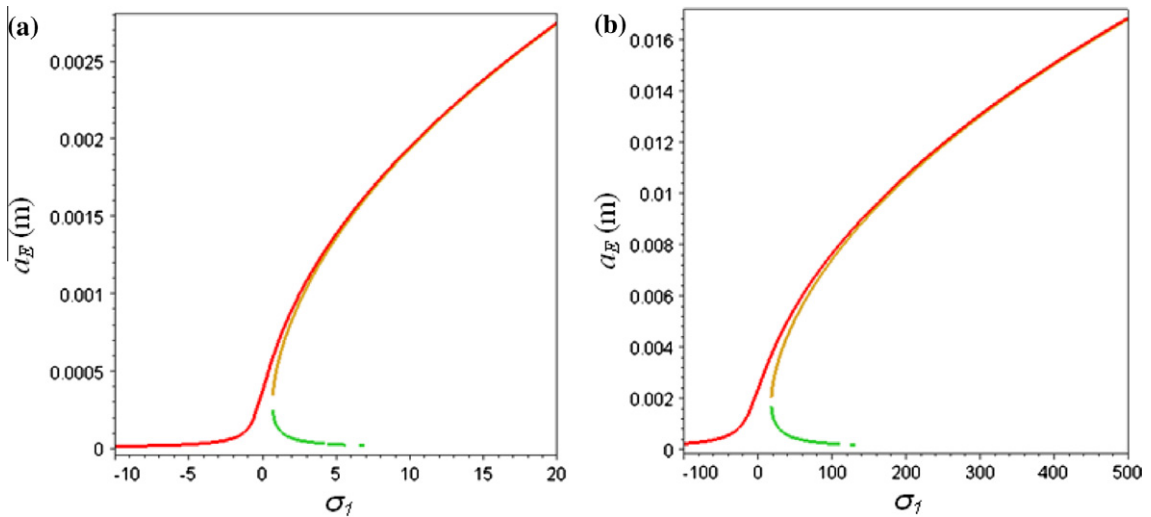

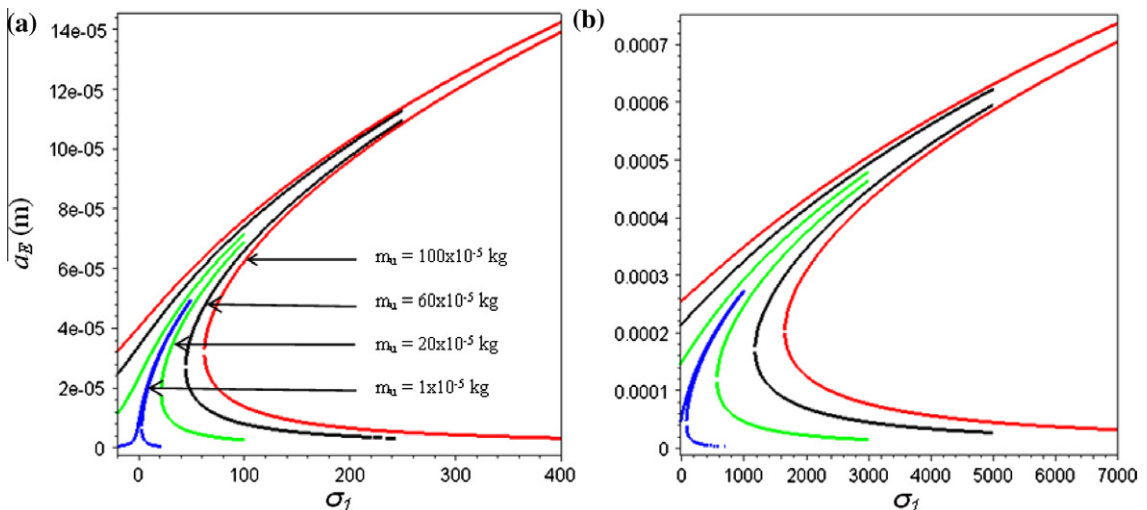**Fig. 7.** Effect of $\beta 2 = 0$ (a) $\Omega = \omega_1$ (b) $\Omega = \omega_2$.

Fig. 8. Effect of variation in mass unbalance m_u (a) $\Omega = \omega_1$ (b) $\Omega = \omega_2$.
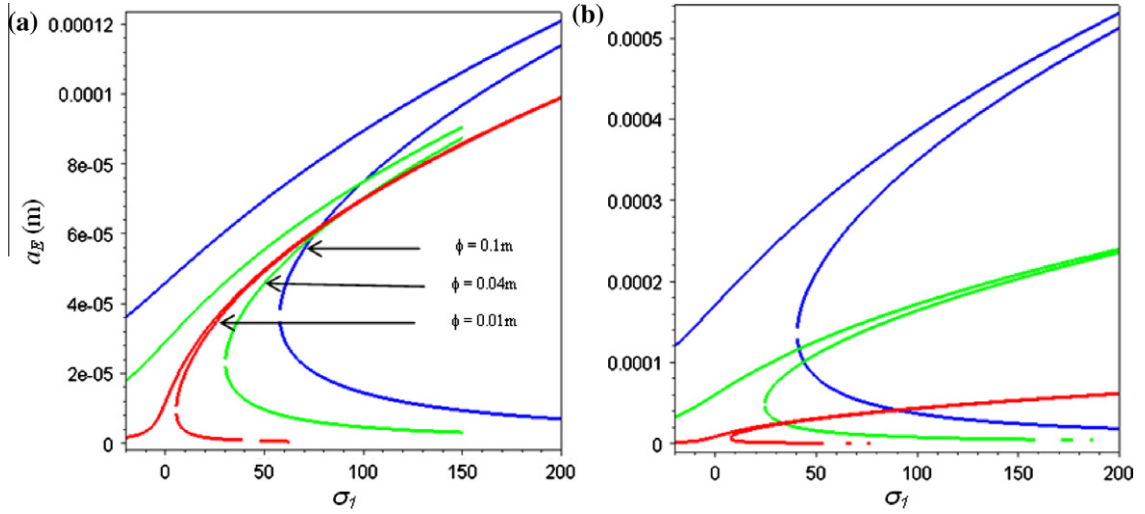
Fig. 9. Effect of variation in shaft diameter (a) $\Omega = \omega_1$ (b) $\Omega = \omega_2$.

numerical solutions of Eq. (34), thus generating different resonant curves. Therefore these different parameters can be adjusted to change the behavior of the rotor significantly.

4.2.1. Effect of $\beta_2 = 0$

According to Eq. (22) quantity β_2 depends on k_3 which represents the effect of an axial dynamic force, see Eq. (11). This implies that if we want to study the dynamics of the system without considering the effect of an axial force we can substitute $\beta_2 = 0$ in various constants given in Appendix B. This affects the overall response of the system. The generated resonant curves are presented in Fig. 7. A comparison of these curves with those of Fig. 2 shows that the amplitude has increased. Also a decrease in the horizontal plotting range of these curves indicates that the spring hardening effect becomes visible even at very low values of detuning parameter σ_1.

4.2.2. Effect of varying the mass unbalance m_u

The quantity d_4 in the polynomial given by Eq. (34) depends on the mass unbalance m_u through Eqs. (B.2) and (B.10) in Appendix B and Eq. (22) in the text. Therefore the response of the system can be varied by changing the value of the mass unbalance. Fig. 8 represents the effect of varying the mass unbalance from 1×10^{-5} kg to 100×10^{-5} kg. Different resonant curves plotted on the same scale show that as the mass unbalance is increased, the horizontal component of these curves expands more to cover a greater range of detuning parameter σ_1.

4.2.3. Effect of varying shaft cross-sectional radius R_1

The quantities α_1, β_1, α_2, β_2 and m_1 in Appendix B are related to parameters b_1, b_2, k_1, k_2, k_3 using Eq. (22). All these parameters depend on the cross-sectional radius of the shaft. This can be observed from Eqs. (9a), (9b) and (11) in the text and Eqs. (B.12)–(B.16) in Appendix B. Therefore a change in the shaft radius will change the numerical values of all the parameters and quantities mentioned above. Fig. 9 shows the system response for three different values of shaft cross-sectional radius. It can be observed that the resonant curves bend more strongly towards right as the shaft narrows.

5. Conclusions

The nonlinear behavior of rotor dynamics due to large deformations and a dynamic axial force was analysed for the first mode. A mathematical model was developed and solved using the multiple scales method. The numerical investigations were conducted using three methods, i.e. the method of multiple scales, a continuation procedure (Matcont) and a step by step analysis in Matlab Simulink. It is concluded that the method of multiple scales is more efficient than the other two methods as all the stable and unstable solutions can be seen in the resonant curves.

The results showed that nonlinearities along with other phenomena like gyroscopic, rotary inertia and mass unbalance effects significantly influence the dynamics of the rotor system. The linear analysis showed that resonance existed only at the second critical speed, but in the nonlinear analysis another resonance appeared at the first critical speed. Furthermore, nonlinearities caused the resonance curves to be of hard spring type. In the absence of dynamic axial force and at lower values of mass unbalance, the spring hardening effect was visible even at lower values of detuning parameter σ_1. Using the method of analysis presented here facilitated studying the changes caused by modifying different rotor system parameters,

by changing the numerical values of the latter. The future perspectives of this work include the experimental validation of the results and the consideration of the effect of shear deformations (Timoshenko beam).

Appendix A

A.1. Strain energy of the shaft

The shaft is modeled as a beam of circular cross section in bending (Fig. A). The displacements in the x, y and z directions of the beam are given below.

$$u_x = u, \quad u_y = -z\theta_x + x\theta_z, \quad u_z = w. \tag{A.1}$$

The longitudinal strain (deformation) in the y direction can be shown to be

$$\varepsilon_{yy} = \underset{\underset{\varepsilon_l}{\downarrow}}{\overbrace{-z\frac{\partial\theta_x}{\partial y}+x\frac{\partial\theta_z}{\partial y}}} + \underset{\underset{\varepsilon_{nl}\text{(higher order deformations)}}{\downarrow}}{\overbrace{\frac{1}{2}\theta_x^2+\frac{1}{2}\theta_z^2.}} \tag{A.2}$$

The strain energy can be given as:

$$U_s1 = \frac{1}{2}\int_0^L\int_A (\sigma_{yy}\varepsilon_{yy})\,dA\,dy. \tag{A.3}$$

By using the relation $\sigma_{yy} = E\varepsilon_{yy}$, the strain energy can be written as:

$$U_{s1} = \frac{E}{2}\int_0^L\int_A \varepsilon_{yy}^2\,dA\,dy. \tag{A.4}$$

By using Eq. (A.2),

$$U_{s1} = \frac{E}{2}\int_0^L\int_A \left(-z\frac{\partial\theta_x}{\partial y}+x\frac{\partial\theta_z}{\partial y}+\frac{1}{2}\theta_x^2+\frac{1}{2}\theta_z^2\right)^2 dA\,dy, \tag{A.5}$$

$$U_{s1} = \frac{E}{2}\int_0^L\int_A \left[\begin{array}{l} z^2\left(\frac{\partial\theta_x}{\partial y}\right)^2 + x^2\left(\frac{\partial\theta_z}{\partial y}\right)^2 - 2xz\left(\frac{\partial\theta_x}{\partial y}\right)\left(\frac{\partial\theta_z}{\partial y}\right) + \frac{1}{4}\theta_x^4 \\ +\frac{1}{4}\theta_z^4 + \frac{1}{2}\theta_x^2\theta_z^2 - 2\left(z\frac{\partial\theta_x}{\partial y}+x\frac{\partial\theta_z}{\partial y}\right)\left(\frac{1}{2}\theta_x^2+\frac{1}{2}\theta_z^2\right) \end{array}\right] dA\,dy. \tag{A.6}$$

The 3rd and 7th term in the above equation can be neglected due to the symmetry of the cross-section. Also, $I_x = \int_A z^2 dA$, $I_z = \int_A x^2 dA$, $I = I_x = I_z$ (due to symmetry) and $\int_S ds = A$ is the area of the cross section.

Therefore, Eq. (A.6) becomes,

$$U_s1 = \frac{EI}{2}\int_0^L \left[\left(\frac{\partial\theta_x}{\partial y}\right)^2 + \left(\frac{\partial\theta_z}{\partial y}\right)^2\right] dy + \frac{EA}{2}\int_0^L \left[\frac{1}{4}\theta_x^4 + \frac{1}{4}\theta_z^4 + \frac{1}{2}\theta_x^2\theta_z^2\right] dy. \tag{A.7}$$
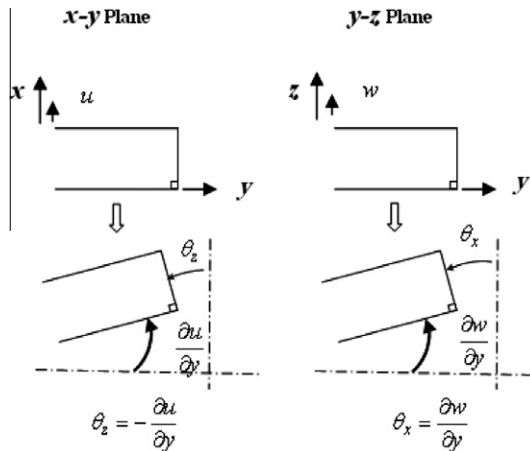

Fig. A. Transverse vibrations (beam in bending).

Appendix B

B.1. Linear analysis

The rotor was studied as a free undamped linear system to determine the natural frequencies of vibration and the Campbell diagram given in Fig. B(a) was plotted to determine the critical speeds. The two critical speeds ω_1 *and* ω_2 were found to be 2520 rpm (42 Hz) and 3089 rpm (51.5 Hz). The response due to mass unbalance is given in Fig. B(b) which shows that there is a peak in the amplitude corresponding to the second critical speed.

B.2. Constants

Different constants incorporated in Eqs. (34) and (35) are given as

$$c_2 = C_2/C_1, \quad c_3 = C_3/C_1, \quad c_5 = C_5/C_1, \tag{B.1}$$

$$d_2 = D_2/D_1, \quad d_3 = D_3/D_1, \quad d_4 = D_4/D_1, \quad d_5 = D_5/D_1, \tag{B.2}$$

where

$$C_1 = -2\omega_1^3 - \alpha_1\omega_1^2\omega_2 + \alpha_1^2\omega_1\omega_2^2 + 2\alpha_2\omega_1 - \alpha_1\alpha_2\omega_2, \tag{B.3}$$

$$C_2 = 2i(\beta_1 + 2\beta_2)(\omega_1^2 + \alpha_1\omega_1\omega_2 - \alpha_2), \tag{B.4}$$

$$C_3 = 4i(\beta_1 + 2\beta_2)(\omega_1^2 + \alpha_1\omega_1\omega_2 - \alpha_2) = 2C_2, \tag{B.5}$$

$$C_5 = -c(\omega_1^3 + \alpha_1\omega_1^2\omega_2 - \alpha_2\omega_1), \tag{B.6}$$

$$D_1 = (-\alpha_1 - \alpha_1^2 + 2)\omega_2^3 - \alpha_2(\alpha_1 + 2)\omega_2, \tag{B.7}$$

$$D_2 = 2i(\beta_1 + 2\beta_2)[(\alpha_1 - 1)\omega_2^2 + \alpha_2], \tag{B.8}$$

$$D_3 = 4i(\beta_1 + 2\beta_2)[(\alpha_1 - 1)\omega_2^2 + \alpha_2] = 2D_2, \tag{B.9}$$

$$D_4 = \frac{1}{2}m_1d_1f(l_1)[(\alpha_1 - 1)\omega_2^4 + \alpha_2\omega_2^2], \tag{B.10}$$

$$D_5 = c[(1 - \alpha_1)\omega_2^3 - \alpha_2\omega_2]. \tag{B.11}$$
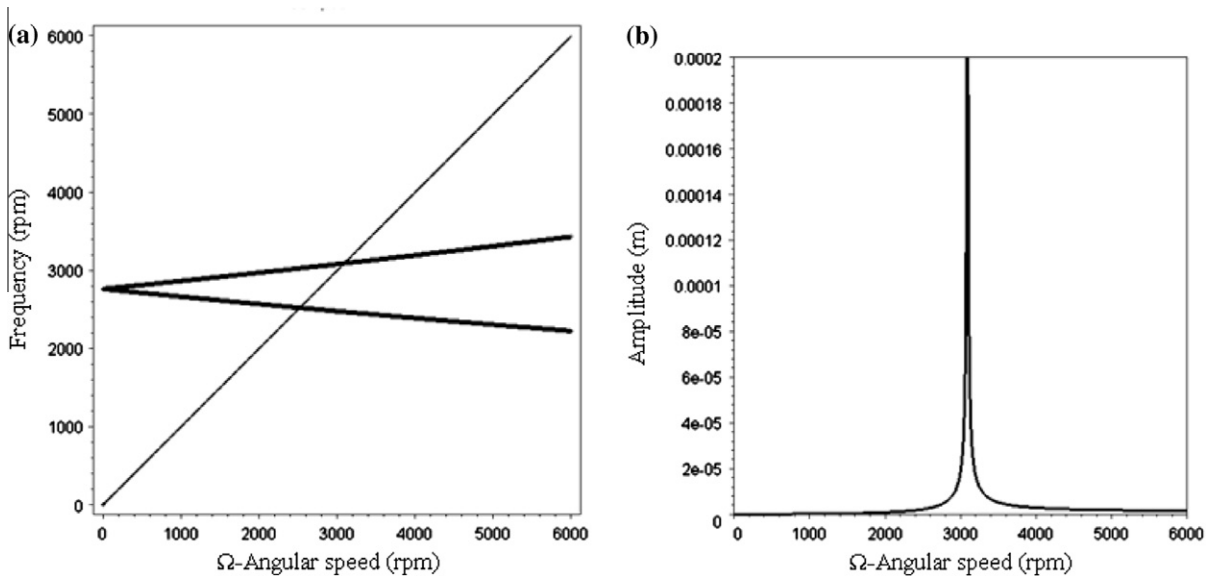

Fig. B. (a) Campbell diagram, (b) mass unbalance response.

B.3. Numerical data

$$\rho = 7800 \text{ kg m}^{-3}, \quad E = 2 \times 10^{11} \text{ N m}^{-2}, \quad c = 0.001, \quad L = 0.4 \text{ m}, \quad R_1 = 0.01 \text{ m},$$

$$R_2 = 0.15 \text{ m}, \quad h = 0.03 \text{ m}, \quad m_u = 1 \times 10^{-4} \text{ kg}, \quad d_1 = R_2 = 0.15 \text{ m},$$

$$M_d = \pi \left(R_2^2 - R_1^2 \right) h\rho = 16.47 \text{ kg,}, \tag{B.12}$$

$$I_{dx} = M_d \left(3R_1^2 + 3R_2^2 + h^2 \right)/12 = 9.427 \times 10^{-2} \text{ kg m}^2, \tag{B.13}$$

$$I_{dy} = M_d \left(R_1^2 + R_2^2 \right)/2 = 1.861 \times 10^{-1} \text{ kg m}^2, \tag{B.14}$$

$$A = \pi R_1^2 = 3.142 \times 10^{-4} \text{ m}^2, \tag{B.15}$$

$$I = \pi R_1^4/4 = 7.854 \times 10^{-9} \text{ m}^4. \tag{B.16}$$

For the geometry and material properties of the rotor system given above, the numerical values of different constants in expressions (B.2)–(B.11) are given as

$$\alpha_1 = 2.0084 \text{x} 10^{-1}, \quad \alpha_2 = 83.623 \text{x} 10^3, \quad \beta_1 = 2.5087 \text{x} 10^9, \quad \beta_2 = 9.5457 \text{x} 10^{12}, \quad \omega_1 = 258,$$

$$\omega_2 = 323, \quad f(l_1) = 8.660 \text{x} 10^{-1}, \quad d_1 = 0.15, \quad c = 0.001.$$

References

[1] T. Yamamoto, Y. Ishida, Linear and Nonlinear Rotordynamics: A Modern Treatment with Applications, Wiley & sons, 2001.
[2] F.F. Ehrich, Handbook of Rotor Dynamics, Krieger, Malabar, 1999.
[3] M. Lalanne, G. Ferraris, Rotordynamics Prediction in Engineering, second ed., John Wiley & sons, 1998.
[4] G. Genta, Dynamics of Rotating Systems, Springer, New York, 2005.
[5] L.M. Adams, J.R. Adama, Rotating Machinery Vibrations from Analysis to Troubleshooting, Dekker, New York, 2001.
[6] R. Sino, T.N. Baranger, E. Chatelet, G. Jacquet, Dynamic analysis of a rotating composite shaft, Composites Science and Technology 68 (2008) 337–345.
[7] F. Ehrich, Observations of nonlinear phenomena in rotordynamics, Journal of system design and dynamics 2 (3) (2008) 641–651.
[8] N. Driot, C.H. Lamarque, A. Berlioz, Theoretical and experimental analysis of a base excited rotor, ASME Journal of Computational and Nonlinear Dynamics, Transaction of ASME 1 (4) (2006) 257–263.
[9] M. Duchemin, A. Berlioz, G. Ferraris, Dynamic behavior and stability of a rotor under base excitations, Journal of Vibration and Acoustics 128 (5) (2006) 576–585.
[10] M. Duchemin, A. Berlioz, G. Ferraris, Etude du comportement dynamique des rotors embarqués: modélisation – expérimentation, ASTE 30 (2004) 27–33.
[11] N. Driot, A. Berlioz, C.H. Lamarque, Stability and stationary response of a skew jeffcott rotor with geometric uncertainty, ASME Journal of Computational and Nonlinear Dynamics, Transaction of ASME 4 (2) (2009).
[12] J. Luczko, A geometrically nonlinear model of rotating shafts with internal resonance and self excited vibrations, Journal of Sound and Vibrations 255 (3) (2002) 433–456.
[13] Z. Xia, G. Qiao, T. Zheng, W. Zhang, Nonlinear modelling and dynamic analysis of the rotor-bearing system, Nonlinear Dynamics 57 (2009) 559–577.
[14] J.C. Ji, A.Y.T. Leung, Nonlinear oscillations of a rotor magnetic bearing system under superharmonic resonance conditions, Internations Journal of Non-linear Mechanics 38 (2003) 829–835.
[15] Y. Ishida, I. Nagasaka, T. Inoue, S. Lee, Forced oscillations of a vertical continuous rotor with geometric nonlinearity, Nonlinear dynamics 11 (1996) 107–120.
[16] M. Geradin, D. Rixen, Theorie Des Vibrations – Application a la Dynamique des Structures, Masson, Paris, 1992.
[17] A.H. Nayfeh, D.T. Mook, Nonlinear Oscillations, Wiley, New York, 1979.
[18] A.H. Nayfeh, Introduction to Perturbation Techniques, Wiley, New York, 1993.
[19] S. Hosseini, S. Khadem, Free vibration analysis of a rotating shaft with nonlinearities in curvature and inertia, Mechanism and Machine theory 44 (2009) 272–288.
[20] G. Michon, L. Manin, R.G. Parker, R. Dufour, Duffing oscillator with parametric excitation: analytical and experimental investigation on a belt-pulley system, Journal of Computational and Nonlinear Dynamics (3) (2008).
[21] H. Yabuno, Y. Kunitho, T. Inoue, Y. Ishida, Nonlinear analysis of rotor dynamics by using method of multiple scales, Iutam Symposium on Dynamics and Control of Nonlinear Systems with Uncertainty 2 (part 3) (2007) 167–176.
[22] A.F. El-Bassiouny, Parametrically excited non-linear systems: a comparison of two models, Applied Mathematics and Computation 132 (2002) 385–410.